Geological Society of America Bulletin

Rapid exhumation and cooling of the Liaonan metamorphic core complex: Inferences from $^{40}Ar/^{39}Ar$ thermochronology and implications for Late Mesozoic extension in the eastern North China Craton

Jin-Hui Yang, Fu-Yuan Wu, Sun-Lin Chung, Ching-Hua Lo, Simon A. Wilde and Gregory A. Davis

Geological Society of America Bulletin 2007;119;1405-1414
doi: 10.1130/B26085.1

Rapid exhumation and cooling of the Liaonan metamorphic core complex: Inferences from $^{40}Ar/^{39}Ar$ thermochronology and implications for Late Mesozoic extension in the eastern North China Craton

Jin-Hui Yang*
Fu-Yuan Wu
State Key Laboratory of Lithospheric Evolution, Institute of Geology and Geophysics, Chinese Academy of Sciences, P.O. Box 9825, Beijing 100029, China

Sun-Lin Chung
Ching-Hua Lo
Department of Geosciences, National Taiwan University, Taipei, Taiwan

Simon A. Wilde
Department of Applied Geology, Curtin University of Technology, Perth, Australia

Gregory A. Davis
Department of Earth Sciences, University of Southern California, Los Angeles, California 90089-0740, USA

ABSTRACT

The Liaonan metamorphic core complex formed during crustal extension in the Liaodong Peninsula, eastern North China craton, and consists of the Jinzhou detachment fault, Proterozoic–Paleozoic sedimentary rocks in its upper plate, and exhumed high-grade Archean metamorphic rocks and Early Cretaceous granitic plutons in the lower plate. Exhumation of its footwall from mid-crustal levels is evidenced in the detachment fault zone by the temporal transition from amphibolite facies mylonitization at depth, through retrograde chloritic shearing and brecciation, to brittle faulting during final uplift. The footwall mylonite zone is 2.5–3.5 km thick and includes Early Cretaceous (128–118 Ma) granitic rocks, together with older metamorphic rocks. The $^{40}Ar/^{39}Ar$ ages of muscovite, hornblende, biotite, and K-feldspar from the mylonitic rocks record that the core complex cooled between ca. 120 and 107 Ma, from the time of initial crystallization of zircons (122–118 Ma) at 700–800 °C in syntectonic leucocratic dikes and granitic rocks, to closure of argon diffusion in hornblende, micas, and K-feldspar at ~500 to ~200 °C. Throughout the eastern North China craton, the synchroneity of cooling and exhumation of metamorphic core complexes, the formation of pull-apart basins, and regional alkaline igneous activity, reflects regional extensional tectonics in the Early Cretaceous. This accompanied lithospheric thinning, possibly resulting from the rollback of the subducted Pacific plate along the eastern Asian margin during the Early Cretaceous.

Keywords: argon thermochronology, metamorphic core complex, crustal extension, Early Cretaceous, North China Craton, Liaodong Peninsula, Liaonan metamorphic core complex.

INTRODUCTION

The late Mesozoic tectonic history of the eastern North China Craton (NCC; Fig. 1) was marked by crustal extension and lithospheric thinning (Menzies et al., 1993; Griffin et al., 1998; Xu, 2001), characterized by widely developed metamorphic core complexes (Fig. 1B) (Yin and Nie, 1996; Davis et al., 2001; Darby et al., 2004; Liu et al., 2005) and pull-apart basins (Meng, 2003), regional A-type granitic magmatism (Fig. 1B) (Wu et al., 2005; Yang et al., 2006a), and large-scale gold mineralization (e.g., Yang et al., 2003).

Crustal extension was greatest within a number of metamorphic core complexes distributed across the North China Craton (Fig. 1B), but was primarily located within the Mesozoic Yanshan fold and thrust belt along the northern edge of the North China craton (Darby et al., 2004) and the Dabie-Sulu orogenic belt at the southern margin of the craton (Zhang et al., 1998). Within the core complexes, mid-crustal crystalline rocks were transported to the surface in the footwalls of what are now, and may have been then, shallow-dipping master extensional detachment faults. The Liaonan metamorphic core complex of eastern Liaoning is the easternmost recognized core complex in the North China craton (Yang et al., 1996; Liu et al., 2005). Its west-northwest–rooting master detachment is the Jinzhou fault, which juxtaposes an upper plate of Proterozoic–Paleozoic sedimentary rocks against a lower plate of high-grade Archean metamorphic rocks and Early Cretaceous granitic plutons. The Liaonan metamorphic core complex is typical of Cordilleran-style metamorphic core complexes in that the Jinzhou detachment fault is above a thick, well-developed zone of amphibolite-grade mylonitic gneisses that overprinted Archean protoliths and synextensional Cretaceous plutons. The mylonitic rocks were overprinted at higher structural levels by retrograde metamorphism (e.g., chloritization), brittle shearing, and cataclasis. The footwall records the progressive uplift and fault-related deformation under increasingly shallower and cooler crustal conditions and in this respect is identical

*Corresponding author: Jin-Hui Yang, +86-10-62007900, jinhui@mail.igcas.ac.cn

GSA Bulletin; November/December 2007; v. 119; no. 11/12; p. 1405–1414; doi: 10.1130/B26085.1; 5 figures; 1 table.

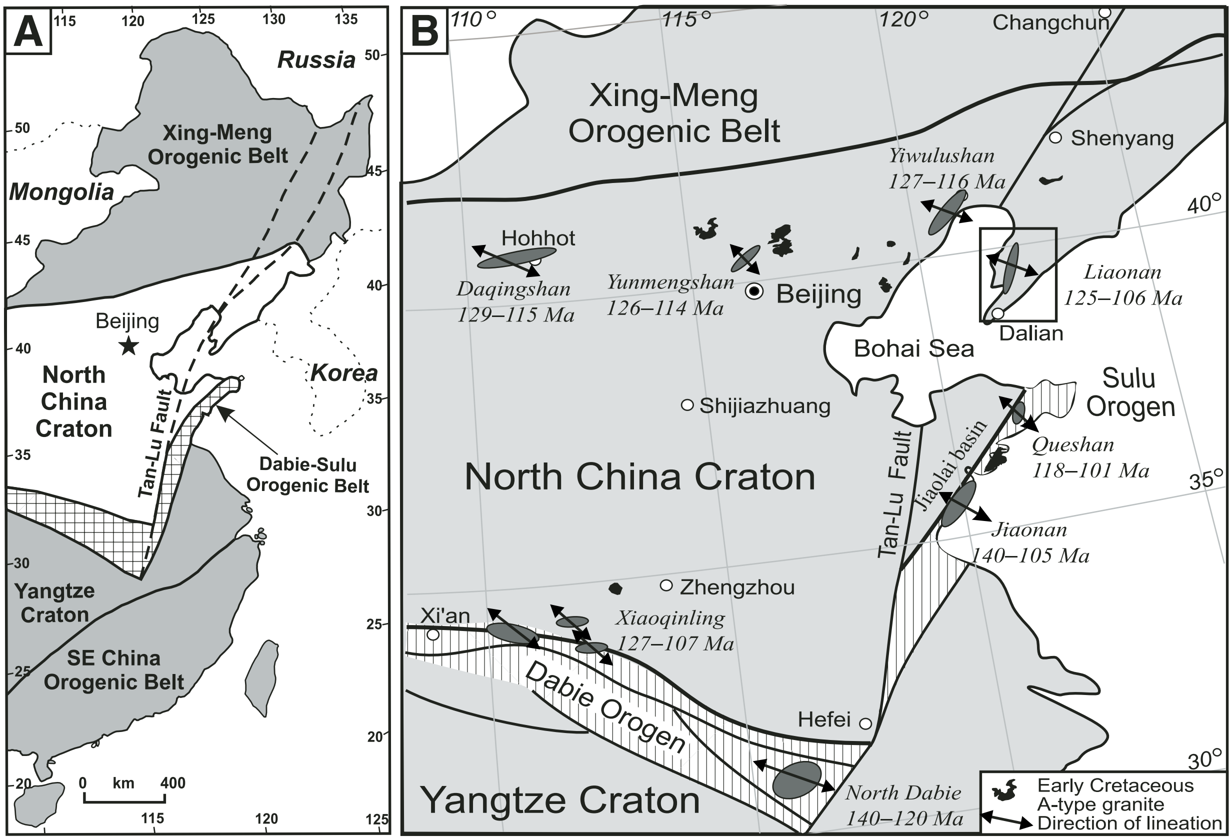

Figure 1. (A) Simplified geological map of eastern China, showing main tectonic elements. (B) Geological sketch map of the eastern North China craton showing locations of A-type granites and metamorphic core complexes with recent data on the age and kinematics of Early Cretaceous deformation (see text for references). Rectangle shows the location of the study area in the Liaodong Peninsula.

to that seen in Cordilleran metamorphic core complexes in the southwestern U.S. (e.g., Lister and Davis, 1989).

Previous studies have described detailed geometric and kinematic aspects of the Liaonan metamorphic core complex (e.g., Xu et al., 1991; Zhang and Wang, 1995; Yang et al., 1996; Yin and Nie, 1996; Chen et al., 1999; Gang et al., 1999; Liu et al., 2005); however, the timing of the tectonic exhumation of the lower plate is poorly constrained. This paper presents new results from a detailed $^{40}Ar/^{39}Ar$ thermochronological investigation using a suite of minerals with different closure temperatures (T_c) to determine the cooling history of the lower plate. The comparison of these new data with previously published geochronological data (Wu et al., 2005) and structural analysis (Yang et al., 1996; Liu et al., 2005) enables a reconstruction of the thermal evolution of the Liaonan metamorphic core complex as its footwall metamorphic and mylonitic rocks were transferred upward from the brittle-ductile transition in a very short period of time (120–107 Ma). The coeval formation of widespread metamorphic core complexes, pull-apart basins, and regional alkali magmatism indicates large-scale extension in the eastern North China craton; the extension was related to lithospheric thinning, possibly the result of the rollback of the subducted Pacific plate along the eastern Asian margin during the Early Cretaceous.

GEOLOGY OF THE LIAONAN METAMORPHIC CORE COMPLEX

Eastern China is composed of the accretionary Xing'an-Mongolia (Xing-Meng) orogenic belt in the north, the North China craton to the south, and the Dabie-Sulu ultrahigh-pressure orogenic belt farther to the south and east (Fig. 1A; Wang and Mo, 1996). The Archean basement of the North China craton is the oldest tectonic unit in China (as old as 3.8 Ga; Liu et al., 1992) and is characterized by the widespread distribution of Neoarchean tonalite-trondhjemite-granodiorite (TTG) suites, with minor amounts of supracrustal rocks. The craton was stabilized during the Paleoproterozoic and subsequently covered by a thick sequence of Proterozoic–Paleozoic sediments (Zhao et al., 2001). However, more recent studies have demonstrated that at least parts of the northern edge of the craton were the site of a Paleozoic Andean-type plate margin with extensive igneous intrusion and metamorphism accompanying the southward subduction of Mongolian oceanic terranes beneath the continent (Zhang et al., 2006; Yang et al., 2006b). Final amalgamation of the Mongolian terranes and the North China craton occurred in the Permian. The North China craton thus had a protracted and complicated Paleozoic–Mesozoic history of magmatism, metamorphism, thrusting of basement and cover rocks, and finally regional extensional overprinting in the Early Cretaceous, the subject of this paper.

The Liaonan metamorphic core complex is located east of the Tan-Lu fault on the Liaodong Peninsula of the eastern North China craton (Fig. 1B). Its main structural element is the Jinzhou low-angle extensional detachment fault that separates largely supracrustal rocks ranging in age from Neoproterozoic to Cretaceous from a lower plate of Neoarchean to Cretaceous crystalline rocks exhumed from mid-crustal depths (Fig. 2A; Xu et al., 1991; Yin and Nie, 1996; Liu et al., 2005).

Lithologies of the Lower Plate of the Liaonan Complex

The lower plate contains Neoarchean–Paleoproterozoic gneisses, Paleoproterozoic Liaohe Group schists, and Early Cretaceous granitic plutons. The Neoarchean to Paleoproterozoic gneisses are composed of TTG rocks metamorphosed to amphibolite or granulite facies. Laser ablation-inductively coupled plasma-mass spectrometer (LA-ICP-MS) U-Pb analyses of zircon from the TTG gneisses reveal a range of ages from 2518 to 2457 Ma (Lu et al., 2004). The Paleoproterozoic strata of the Liaohe Group are mostly pyroclastic rocks of intermediate to felsic composition and clastic sediments and carbonates that underwent greenschist to amphibolite facies metamorphism between 2.17 and 1.93 Ga (Luo et al., 2004). The presumed unconformity between the Liaohe Group and Archean basement gneisses is not exposed.

Early Cretaceous plutonic rocks were intruded into what are now the lower plate basement rocks (Fig. 2A). They are mainly composed of porphyric granodiorite and medium- to fine-grained monzogranite, with lesser amounts of monzodiorite and diorite. Field observations, petrography, and geochemistry indicate that the monzogranite and its dioritic enclaves were mainly derived from partial melting of lower crustal materials, but with some involvement of mantle-derived melts via a complex process including magma mixing, crustal anatexis, and crystal fractionation, whereas the granodiorites were mainly derived from partial melting of the lower crust (Yang et al., 2004, 2007).

Jinzhou Detachment Fault

The Jinzhou detachment fault (Fig. 2A) borders the western and southern margins of the Liaonan metamorphic core complex. The fault zone has an arcuate antiformal map trace as the result of post-extensional folding of the core complex (Fig. 2A). Its western segment strikes north-northwest and dips west-northwest, whereas its southern segment strikes east-northeast and dips south-southeast (Fig. 2). The brittle Jinzhou fault reactivated a fault-related deformation zone that shows characteristics of progressive ductile to brittle development. Thick mylonitic gneisses in the footwall are kinematically related to the Jinzhou fault and formed in a deep crustal ductile shear zone, in which quartz deformed crystal-plastically while other minerals, e.g., feldspar and hornblende, were deforming brittlely. The protoliths of these mylonitic rocks, which form a section 2–3.5 km thick, were Archean and Proterozoic crystalline units, as well as Cretaceous plutons emplaced both into and below the ductile shear zone. Upward transport of amphibolite-grade mylonitic gneisses in the footwall of the Jinzhou fault led to their progressive retrogression to greenschist facies assemblages, to increasingly brittlely sheared and retrograde mylonitic rocks closest to the detachment fault (chloritic breccias), and to pure cataclasites (including microbreccias; Figs. 3A–3C) in a zone of variable thickness directly below the fault. This pattern of progressive overprinting of hotter, ductilely deformed rock assemblages and fabrics during increasingly colder and shallower brittle retrogression and cataclasis is typical of the footwalls of metamorphic core complexes (Davis and Lister, 1988; Lister and Davis, 1989).

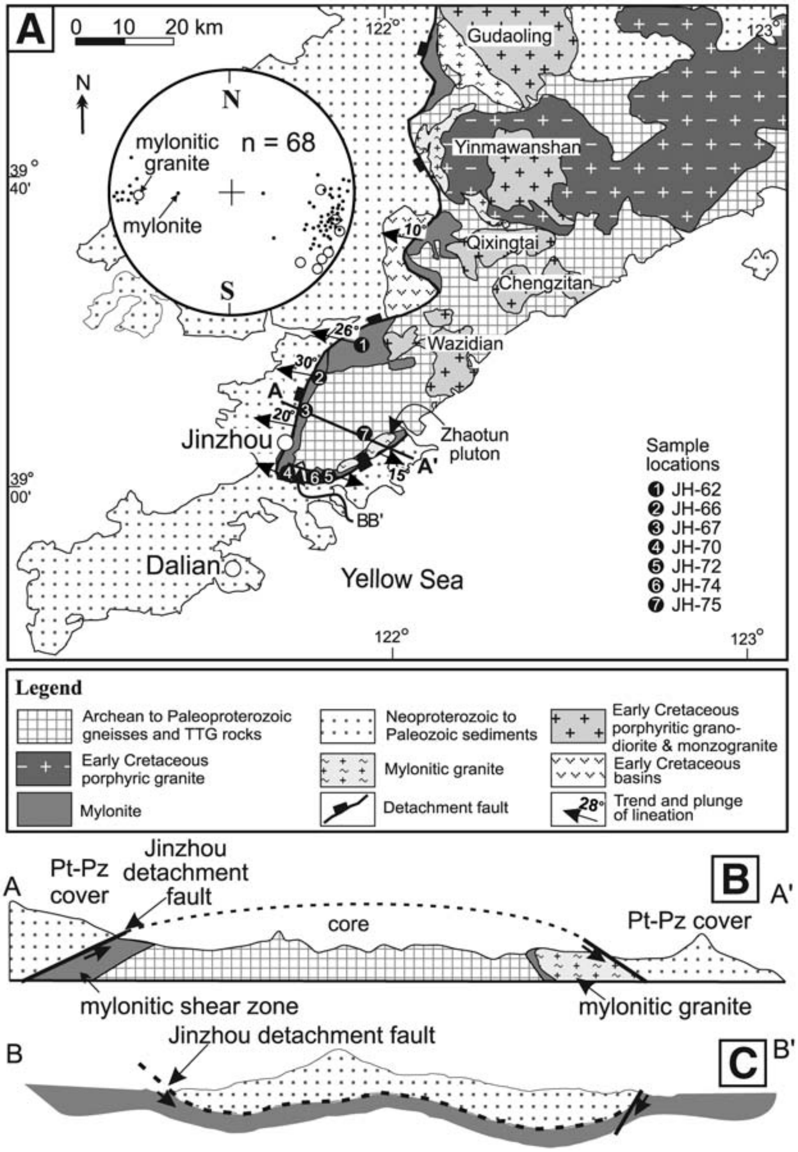

Figure 2. (A) Geological map of the Liaonan metamorphic core complex in the Liaodong Peninsula. Inset is an equal-area lower hemisphere projection of stretching lineations in mylonitic gneiss and granite. TTG—tonalite-trondhjemite-granodiorite. (B) Geological cross section showing the spatial relationship of the detachment fault and the metamorphic core complex. Pt-Pz—Proterozoic–Paleozoic. (C) Geological section across the allochthonous block (Neoproterozoic–Paleozoic sedimentary block that has been moved from its original site of formation by low-angle thrust faulting) bounded by the detachment fault zone.

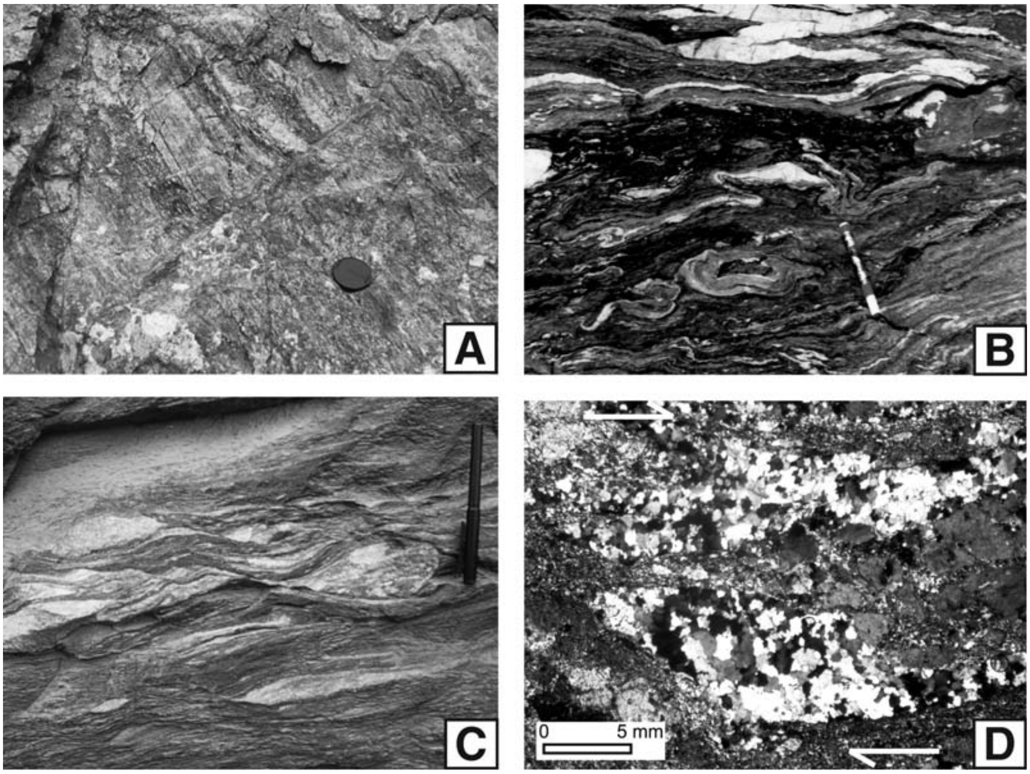

Figure 3. Photographs showing structural and microstructural characteristics of deformed rocks from the Liaonan metamorphic core complex. (A) Cataclastic zones; lens cap is 8.5 cm in diameter. (B) Sheath fold in the lower plate; pen is 14 cm long. (C) Mylonite; pen is 14 cm long. (D) Thin section of mylonite microstructure.

The thickness of retrograded and cataclastic mylonitic rocks varies from several hundreds of meters to as much as a kilometer.

Deformation Structures in Fault-Related Lower Plate Rocks

Structures and microstructures of the dynamically recrystallized mylonitic rocks provide evidence that their deformation was produced by ductile flow within a deep shear zone (Figs. 3A–3D). The main deformation mechanism in the mylonitic gneiss was intracrystalline slip of quartz, followed by recovery and recrystallization (Fig. 3D). Dynamic recrystallization in quartz in the mylonitic gneiss occurred at temperatures >300 °C, whereas in feldspar, this mechanism is important only above 450–500 °C (Passchier and Trouw, 1998). Deformation temperatures and the presence of newly formed metamorphic minerals (i.e., Hb + Pl + Q + Bi, Pl + Epi + Q + Bi + Mu, Bi + Mu + Pl + Q and Bi + Mu + Q + Chl; Hb—hornblende, Pl—plagioclase, Q—quartz, Bi—biotite, Epi—epidote, Mu—muscovite, Chl—chlorite) suggest that amphibolite facies conditions prevailed during the dynamic metamorphic event.

Foliation in the mylonite zone, defined by deformed quartz grains, aligned feldspar porphyroclasts, and micas (Fig. 3C), strikes north-northeast (NNE) and dips 10°–30°S southward in the southern part of the core complex, and strikes NNE and dips 2°–50° westward in the western part. Stretching lineations plunge to ~310°, typically at low angles in the western part of the detachment fault zone, and to ~130°, also at low angles, in the southern zone. Sheath and rootless folds, boudinage, and folded boudins are common in the shear zone. Sheath folds have a tubular shape with the hinges parallel to the lineation (Fig. 3B). Mesoscopic structures, most notably S-C fabrics (Fig. 3C) and outcrop-scale normal faults are consistent in indicating a top-to-the-west-northwest shear sense within the footwall fault zone. Kinematic indicators thus confirm that the Jinzhou normal fault roots westward, an unusual geometry for the North China block, but not a unique one; the recently discovered master detachment fault of the Waziyu metamorphic core complex in the Yiwulüshan, western Liaoning, roots in the same direction (Darby et al., 2004).

Synkinematic (Synextensional) Plutons

Syntectonic intrusions are important components of the Liaonan lower plate (Fig. 2A). They are typically in either direct contact with the Jinzhou detachment fault or are in close proximity to it. These intrusions were emplaced at 125–118 Ma (U-Pb zircon ages; Guo et al., 2004; Wu et al., 2005).

A typical example of a major syntectonic intrusion in the metamorphic core complex is the multiple-stage Yimawanshan granodiorite-monzogranite batholith (Fig. 2A; Guo et al., 2004). Two zones are recognized in the batholith—an early marginal zone of porphyritic granodiorite and monzogranite, and a younger inner zone of medium-grained monzogranite. Biotite grains in the inner zone do not have a strong orientation and only a weakly developed foliation of magmatic origin is present; other inner zone mineral grains do not show obvious characteristics of intracrystalline deformation. The magmatic foliation in the inner zone and the inner zone–outer zone boundary generally have high dip angles (~60°–80°), suggesting subvertical emplacement. In the marginal zone, coarse platy plagioclase grains (as long as 5 cm) are oriented and define a primary magmatic foliation and lineation. Hornblende grains or grain aggregates are also strongly orientated (Guo et al., 2004). The degree of orientation is closely related to the proximity of the rocks to the detachment fault zone; i.e., a transition from magmatic fabric to mylonitic orientation (Fig. 2A, inset) is observed when approaching the detachment zone. In addition, the small Zhaotun pluton (Fig. 2A) is spatially controlled, affected by the fault zone, and is characterized by strong foliations and lineations.

Granodiorites in the Zhaotun pluton and in the margins of the Gudaoling and Yinmawanshan batholiths (Fig. 2A) are deformed and exhibit a strong mylonitic foliation. The foliation is defined by the preferred orientation of biotite and feldspar and its intensity increases structurally upward within the plutons. These fabrics are comparable to those of the adjacent country-rock mylonitic gneisses within the Jinzhou shear zone. Microscopic structures, including S-C fabrics, biotite fish, asymmetric porphyroclasts, oblique quartz grain-shape foliation (Fig. 3), and stretching lineations are consistent in indicating a top-to-the-northwest sense of shear (Fig. 2A, inset).

It is significant that magmatic lineations in the intrusions have consistent west-northwest–east-southeast orientations that are parallel to the stretching lineations in the overlying detachment fault rocks (Fig. 2D). This parallelism suggests syntectonic emplacement (Fowler and Paterson, 1997), i.e. magmatic flow in the lower plate may have been influenced by relative slip between the upper plate and the igneous melt below it. Accordingly, we believe, as did Guo et al. (2004), that the Yinmawanshan batholith was a synkinematic pluton (Fig. 2A).

Upper Plate Supra-Detachment Basin

A Cretaceous extensional basin in the upper plate above the western segment of the Jinzhou fault occupies an area of ~93 km^2 (Fig. 2A). Strata in this half-graben basin dip eastward toward the Jinzhou fault; the western margin of the basin is an unconformity between basin strata and underlying Proterozoic sedimentary and volcanic rocks (Liu et al., 2005). Sedimentary rocks in the basin contain Cretaceous fossils, e.g., *Dictyozamites*, *Cycadolepis*, *Elatocladus*, and *Otozamites* (Liaoning Bureau of Geology and Mineral Resources [LBGMR], 1989), supporting an Early Cretaceous age of deposition. Lacustrine sediments of conglomerate, sandstone, siltstone, shale, and marl are the dominant deposits (LBGMR, 1989). Conglomerate clasts include quartz sandstone, andesite, and limestone derived from nearby Neoproterozoic and Paleozoic units, and schist and gneiss from the lower plate Archean basement.

Previous Geochronology of the Liaonan Metamorphic Core Complex

Yin and Nie (1996) dated several samples collected from the Jinzhou mylonitic rocks by using the $^{40}Ar/^{39}Ar$ method, and obtained ages of 153–147 Ma for muscovites and 113–110 Ma for biotites; however, they reported no detailed description of the samples or their contained minerals. Zeng and Li (1996) reported K-Ar ages of 118–103 Ma for muscovites from the mylonite. Recent U-Pb dating of plutons from the lower plate indicates similar ages for granitic rocks within and outside the mylonitic footwall. Weighted mean $^{206}Pb/^{238}U$ zircon ages analyzed using the LA-ICP-MS U-Pb technique are 128–121 Ma for mylonitic granodiorite and 122–118 Ma for undeformed monzogranite (Guo et al., 2004; Wu et al., 2005), indicating that the intrusions were emplaced at the same time, but not allowing the time of mylonitization to be determined. However, zircons from a nonmylonitic leucogranitic dike that intrudes mylonite and mylonitic monzogranite yield a U-Pb age of 120 ± 4 Ma (Wu et al., 2005). This indicates that mylonitization occurred prior to ca. 120 Ma and that plutonic intrusion and mylonitization were coeval.

$^{40}Ar/^{39}Ar$ THERMOCHRONOLOGY

Potassium-rich minerals have a large range of closure temperature (T_c) with respect to the accumulation of radiogenic argon: hornblende ~500 °C (Harrison, 1981), muscovite ~350 °C (Hames and Bowring, 1994), biotite ~300 °C (Harrison et al., 1985), and K-feldspar, with a range of closure temperatures between ~250 and 200 °C (Lovera et al., 1989). Collection of data from these minerals will allow a cooling history to be elucidated because of these differences in closure temperature. We collected seven samples from the footwall mylonitic rocks of the Liaonan metamorphic core complex. The samples have the same fabrics, all of which are consistent in indicating top-to-the northwest sense of shear. The $^{40}Ar/^{39}Ar$ isotopic analyses were performed on 12 minerals separates from these mylonites. The latitudes and longitudes of the collected samples are listed in Table 1 and their locations are shown in Figure 2A.

Analytical Procedures

Mineral separates were prepared using conventional heavy liquid and magnetic separation techniques. After sieving, mineral grains in the range of 250–140 µm were ultrasonically cleaned in 0.5N HCl, washed with distilled water, dried, and hand-picked to remove any visible contamination.

Samples for $^{40}Ar/^{39}Ar$ analysis were irradiated in the VT-c position at the THOR Reactor in Taiwan for 30 h. In order to monitor the neutron flux in the reactor, two aliquots of the LP-6 standard were stacked along with the samples in each irradiation. Standards and samples were either incrementally heated or totally fused using a double-vacuum resistance furnace and/or a U.S. LASER Nd-YAG laser operated in continuous mode; the gas was measured using a VG-3600 mass spectrometer at the National Taiwan University. J values were calculated using argon compositions of the LP-6 biotite standard with an $^{40}Ar/^{39}Ar$ age of 128.4 ± 0.2 Ma (Renne et al., 1998). Ages were calculated from Ar isotope ratios measured after corrections made for mass discrimination, interfering nuclear reactions, decay of ^{39}Ar and ^{37}Ar isotopes, procedural blanks, and atmospheric Ar contamination. Total gas ages were calculated from the sum total of the argon compositions of all temperature steps. Plateau ages were calculated by the same approach, but utilizing only the adjacent temperature steps yielding dates that are concordant with each other within 2σ and including at least 60% of the ^{39}Ar in three or more contiguous steps. Data were then plotted on age spectra and inverse isochron diagrams. The intercept dates and $^{40}Ar/^{36}Ar$ intercept values were calculated from the intercept of the regressed line. The cubic least-square fitting scheme was employed in regressing the data. Because the $^{39}Ar_K$, $^{38}Ar_{Cl}$, and $^{37}Ar_{Ca}$ release data potentially reflect the chemical compositions of the samples (K, Cl, and Ca, respectively), Ca/K and Cl/K ratios were calculated according to the relationships $Ca/K = 3.319 (\pm 0.17) \times {}^{37}Ar_{Ca}/{}^{39}Ar_K$ and $Cl/K = 0.22 (\pm 0.04) \times {}^{38}Ar_{Cl}/{}^{39}Ar_K$, obtained from the analyses of irradiated salts.

Sample Descriptions and Analytical Results

Detailed analytical results of the $^{40}Ar/^{39}Ar$ experiments are given in the GSA Data Repository[1] and summarized in Table 1. The data are also plotted graphically as age spectra and in isotope correlation diagrams in Figure 4. The errors given in Table 1 are at 2σ, whereas those plotted in the Figure 4 are at 1σ. The preferred ages of each sample are also listed in Table 1 on the basis of mean square of weighted deviates (MSWD) assessment according to Wendt and Carl (1991).

Samples JH-62 and JH-75 are from mylonitized amphibolite boudins in the granitic mylonites. They have a granoblastic to lepidoblastic texture, with layers of hornblende and biotite alternating with layers of quartz and plagioclase. Quartz shows undulose extinction and is stretched in the axial plane of a minor fold at the scale of the thin section (Fig. 3D). Hornblende and biotite were obtained from mylonitized amphibolite

[1]GSA Data Repository item 2007258, additional data on the Liaonian metamorphic core complex, is available online at www.geosociety.org/pubs/ft2007.htm. Requests may also be sent to editing@geosociety.org.

TABLE 1. SUMMARY OF $^{40}Ar/^{39}Ar$ DATING RESULTS

Sample no.	Latitude/ longitude	Rock type	Mineral[†]	TGA (Ma)	Mean age[#] (Ma)	Plateau			Isotope correlation		
						Age[#] (Ma)	Steps ^{39}Ar	MSWD	Age (Ma)	$^{40}Ar/^{36}Ar$	MSWD
JH-62	39°19.20′N/ 121°55.62′E	Deformed mafic dike	Hornblende[†]	118.3 ± 1.3	–	113.9 ± 1.6	3–11; 81.1%	0.90	111.8 ± 2.9	1018 ± 730	0.93
			Biotite	112.3 ± 1.3	112.6 ± 0.9	–	_	–	112.4 ± 3.1	309 ± 34	2.4
JH-66		TTG mylonite	Biotite	113.1 ± 1.3	113.3 ± 0.8	–	–	–	114.0 ± 3.0	287 ± 15	1.8
JH-67	39°17.59′N/ 121°51.89′E	TTG mylonite	Biotite	110.2 ± 1.3	110.6 ± 0.7	–	–	–	110.6 ± 2.9	305 ± 15	1.8
			K-feldspar[§]	11.9 ± 1.3	–	112.0 ± 1.2	1–11; 95.5%	0.82	109.7 ± 5.2	417 ± 170	1.6
JH-70	39°07.38′N/ 121°45.67′E	Bi-Pl gneissic mylonite	Biotite	112.2 ± 1.3	112.3 ± 0.7	–	–	–	112.5 ± 3.0	296 ± 16	1.6
			K-feldspar[§]	117.5 ± 1.4	–	114.2 ± 1.3	3–11; 76.1%	0.93	114.7 ± 6.0	289 ± 66	2.1
JH-72	39°06.80′N/ 121°50.11′E	Bi-Pl gneissic mylonite	Biotite	111.0 ± 1.3	111.4 ± 1.2	–	–	–	109.8 ± 4.5	327 ± 46	4.4
JH-74	39°06.82′N/ 121°49.41′E	Mus-Gt granitic mylonite	Muscovite	110.7 ± 1.3	111.6 ± 1.0	–	–		–	–	–
			K-feldspar[§]	109.2 ± 1.4	–	106.5 ± 1.3	1–7; 60.6%	1.6	108.2 ± 4.4	292 ± 14	2.0
JH-75	39°12.06′N/ 121°55.57′E	Mafic mylonite	Hornblende	112.7 ± 1.3	112.9 ± 0.6	–	–	–	109.9 ± 3.4	375 ± 110	1.4
			Biotite	116.4 ± 0.2	113.3 ± 0.8	–	–	–	113.9 ± 3.0	284 ± 28	1.0

Note: TGA—total gas age; TTG—tonalite-trondhjemite-granodiorite; Bi—biotite; Pl—plagioclase; Mus—muscovite; Gt—garnet; MSWD—mean square of weighted deviates.

[†]Minerals analyzed by the furnace step-heating method.

[§]Minerals analyzed by the laser step-heating method. All others were analyzed by the laser single-grain fusion method. All errors in the table are 2σ.

[#]Preferred cooling ages.

samples (JH-62 and JH-75). Furnace step-heating of JH-62 hornblende produced a plateau age of 113.9 ± 1.6 Ma (MSWD = 0.90), corresponding to 81.1% of the $^{39}Ar_K$ released and including nine steps (Fig. 4A). Regression of the data for these nine steps on an inverse-isotope correlation diagram yielded an intercept age of 111.8 ± 2.9 Ma (Table 1; Fig. 4A), consistent with the plateau age of 113.9 ± 1.6 Ma, within error. Hornblende from JH-75 was analyzed using the laser fusion method. Analyses of 20 grains gave a weighted mean $^{39}Ar/^{40}Ar$ age of 112.9 ± 0.6 Ma (n = 20; MSWD = 0.75) and an isochron age of 109.9 ± 3.4 Ma with an initial $^{40}Ar/^{36}Ar$ value that is close to the atmospheric value (Table 1; Fig. 4B). Biotites from samples JH-62 and JH-75 were analyzed by the laser-fusion technique. Sample JH-62 biotite gave a weighted mean age of 112.6 ± 0.9 Ma (n = 18; MSWD = 1.4) and an isochron age of 112.4 ± 3.1 Ma with a $^{40}Ar/^{36}Ar$ value of 309 ± 34 and an MSWD of 2.4 (Table 1; Fig. 4C). Biotite laser-fusion analyses from sample JH-75 resulted in apparent ages ranging from 112.2 to 129.7 Ma. When the laser-fusion data of each sample were plotted on a probability density diagram, two groups of ages were defined (Fig. 4D). Regression of data from the younger group produces an isochron age of 113.9 ± 3.0 Ma (n = 12; MSWD = 1.0) and near-atmospheric initial $^{40}Ar/^{36}Ar$ ratios, consistent with the weighted mean age of 113.3 ± 0.8 Ma (n = 12; MSWD = 0.56) (Table 1; Fig. 4D).

Samples JH-70, JH-72, and JH-74 are mylonitic granitic gneisses. JH-70 and JH-72 contain biotite, K-feldspar, plagioclase, and quartz, whereas JH-75 contains biotite, K-feldspar, and garnet. Most of the laser-fusion analyses of muscovite from sample JH-74 were extremely radiogenic and did not define a linear regression. A probability density plot shows that 14 of 19 analyses form a coherent group and yield a weighted mean age of 111.6 ± 1.0 Ma (n = 14; MSWD = 1.4) (Table 1; Fig. 4E). Biotite laser-fusion analyses of samples JH-70 and JH-72 produced isochron ages of 112.5 ± 3.0 Ma (n = 20; MSWD = 1.6) and 109.8 ± 4.5 Ma (n = 20; MSWD = 4.4), respectively, and near-atmospheric initial $^{40}Ar/^{36}Ar$ ratios, which are consistent with their respective weighted mean ages of 112.3 ± 0.7 Ma (n = 20; MSWD = 0.83) and 111.4 ± 1.2 Ma (n = 20; MSWD = 2.8) (Table 1; Figs. 4F, 4G). K-feldspar was analyzed from mylonitic samples JH-70 and JH-74. K-feldspar release spectra for sample JH-70 records a

Figure 4. $^{40}Ar/^{39}Ar$ data for minerals from lower footwall mylonitic rocks of the Liaonan metamorphic core complex. MSWD—mean square of weighted deviates; Hb—hornblende; Bi—biotite; Kf—potassium feldspar; Mus—muscovite; t—time. (A) Release spectrum and inverse isotope correlation diagrams for hornblende from sample JH-62 analyzed by the furnace step-heating method. (B) Inverse isotope correlation and weighted mean age diagrams for hornblende from sample JH-75 analyzed by laser single-grain fusion technique. (C) Inverse isotope correlation and weighted mean age diagrams for biotite from sample JH-62 analyzed by laser single-grain fusion technique. (D) Inverse isotope correlation and probability density diagrams for biotite from sample JH-75 analyzed by laser single-grain fusion technique. The solid circles in the isochron calculation are from the results shown in the probability density plot. (E) Weighted mean age diagram for muscovite from JH-74 analyzed by laser single-grain fusion technique. (F) Inverse isotope correlation and weighted mean age diagrams for biotite from sample JH-70 analyzed by laser single-grain fusion technique. (G) Inverse isotope correlation and weighted mean age diagrams for biotite from sample JH-72 analyzed by laser single-grain fusion technique. (H) $^{40}Ar/^{39}Ar$ age spectra and isotope correlation diagrams for K-feldspar from sample JH-70 analyzed by the laser step-heating method. (I) $^{40}Ar/^{39}Ar$ age spectra and isotope correlation diagrams for K-feldspar from sample JH-74 analyzed by the laser step-heating method. (J) Inverse isotope correlation and weighted mean age diagrams for biotite from sample JH-66 analyzed by laser single-grain fusion technique. (K) Inverse isotope correlation and weighted mean age diagrams for biotite from sample JH-67 analyzed by laser single-grain fusion technique. (L) $^{40}Ar/^{39}Ar$ age spectra and isotope correlation diagrams for K-feldspar from sample JH-67 analyzed by the laser step-heating method. The errors are plotted at 1σ.

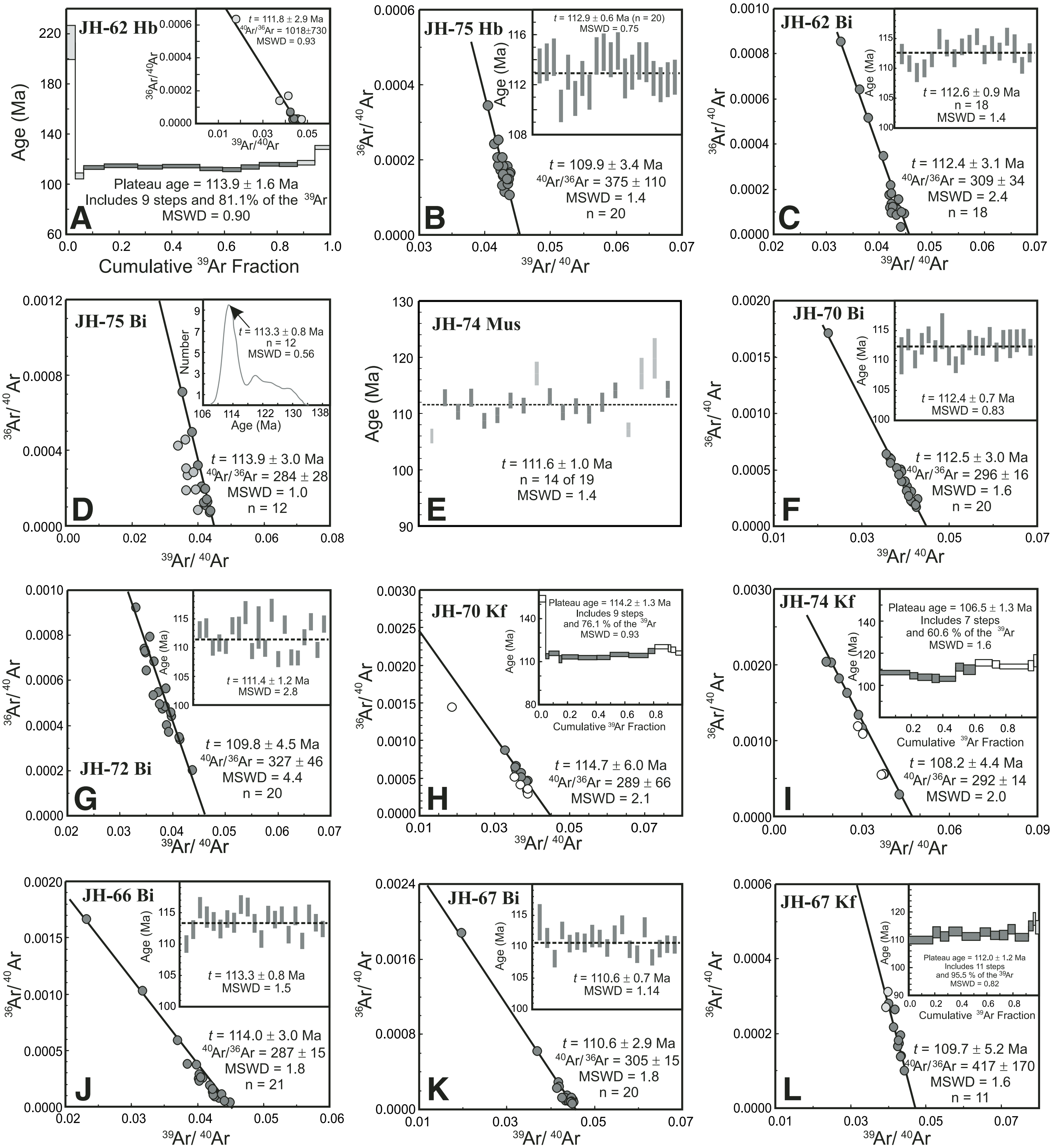
JH-62 Hb
Age (Ma)
Cumulative 39Ar Fraction
t = 111.8 ± 2.9 Ma
40Ar/36Ar = 1018±730
MSWD = 0.93
36Ar/40Ar
39Ar/40Ar
Plateau age = 113.9 ± 1.6 Ma
Includes 9 steps and 81.1% of the 39Ar
MSWD = 0.90
A
JH-75 Hb
t = 112.9 ± 0.6 Ma (n = 20)
MSWD = 0.75
t = 109.9 ± 3.4 Ma
40Ar/36Ar = 375 ± 110
MSWD = 1.4
n = 20
B
JH-62 Bi
t = 112.6 ± 0.9 Ma
n = 18
MSWD = 1.4
t = 112.4 ± 3.1 Ma
40Ar/36Ar = 309 ± 34
MSWD = 2.4
n = 18
C
JH-75 Bi
Number
Age (Ma)
t = 113.3 ± 0.8 Ma
n = 12
MSWD = 0.56
t = 113.9 ± 3.0 Ma
40Ar/36Ar = 284 ± 28
MSWD = 1.0
n = 12
D
JH-74 Mus
t = 111.6 ± 1.0 Ma
n = 14 of 19
MSWD = 1.4
E
JH-70 Bi
t = 112.4 ± 0.7 Ma
MSWD = 0.83
t = 112.5 ± 3.0 Ma
40Ar/36Ar = 296 ± 16
MSWD = 1.6
n = 20
F
JH-72 Bi
t = 111.4 ± 1.2 Ma
MSWD = 2.8
t = 109.8 ± 4.5 Ma
40Ar/36Ar = 327 ± 46
MSWD = 4.4
n = 20
G
JH-70 Kf
Plateau age = 114.2 ± 1.3 Ma
Includes 9 steps
and 76.1 % of the 39Ar
MSWD = 0.93
t = 114.7 ± 6.0 Ma
40Ar/36Ar = 289 ± 66
MSWD = 2.1
H
JH-74 Kf
Plateau age = 106.5 ± 1.3 Ma
Includes 7 steps
and 60.6 % of the 39Ar
MSWD = 1.6
t = 108.2 ± 4.4 Ma
40Ar/36Ar = 292 ± 14
MSWD = 2.0
I
JH-66 Bi
t = 113.3 ± 0.8 Ma
MSWD = 1.5
t = 114.0 ± 3.0 Ma
40Ar/36Ar = 287 ± 15
MSWD = 1.8
n = 21
J
JH-67 Bi
t = 110.6 ± 0.7 Ma
MSWD = 1.14
t = 110.6 ± 2.9 Ma
40Ar/36Ar = 305 ± 15
MSWD = 1.8
n = 20
K
JH-67 Kf
Plateau age = 112.0 ± 1.2 Ma
Includes 11 steps
and 95.5 % of the 39Ar
MSWD = 0.82
t = 109.7 ± 5.2 Ma
40Ar/36Ar = 417 ± 170
MSWD = 1.6
n = 11
L

plateau age of 114.2 ± 1.3 Ma, including nine steps and 76.1% ^{39}Ar, whereas sample JH-74 records a plateau age of 106.5 ± 1.3 Ma, including 7 steps and 60.6% ^{39}Ar (Table 1; Figs. 4H, 4I). Their intercept ages are 114.7 ± 6.0 Ma (MSWD = 2.1) and 108.2 ± 4.4 Ma (MSWD = 2.0), respectively, with near-atmospheric initial ^{40}Ar/^{39}Ar values (Figs. 4H, 4I).

Samples JH-66 and JH-67 are mylonitized Late Jurassic granodioritic and dioritic rocks (Wu et al., 2005) that contain biotite, K-feldspar, plagioclase, and quartz. Biotite from both samples was analyzed by the laser-fusion technique and yielded weighted mean ages of 113.3 ± 0.8 Ma (n = 21; MSWD = 1.5) for JH-66 and 110.6 ± 0.7 Ma (n = 20; MSWD = 1.14) for JH-67, with isochron ages of 114.0 ± 3.0 Ma (n = 21; MSWD = 1.8) and 110.6 ± 2.9 Ma (n = 20; MSWD = 1.8), respectively, and initial ^{40}Ar/^{36}Ar values that are close to atmospheric (Table 1; Figs. 4J, 4K). K-feldspar was analyzed from mylonitic sample JH-67, giving a plateau age of 112.0 ± 1.2 Ma (11 steps and 95.5% ^{39}Ar) and an isochron age of 109.7 ± 5.2 Ma (n = 11; MSWD = 1.6) with a near-atmospheric initial ^{40}Ar/^{39}Ar value (Table 1; Fig. 4L).

DISCUSSION

Timing of Exhumation and Cooling of the Liaonan Metamorphic Core Complex

The zircon U-Pb dating shows that the ages of the mylonitic footwall granodiorites are between 128 and 121 Ma and the ages of the underlying undeformed monzogranites are between 122 and 118 Ma (Guo et al., 2004; Wu et al., 2005). A nondeformed leucosome dike that intruded mylonitic Yinmawanshan medium-grained monzogranite has a zircon U-Pb age of 120 ± 4 Ma (Wu et al., 2005). Collectively, these ages indicate that the onset of formation of the Liaonan metamorphic core complex was ca. 120 Ma.

Hornblende ^{40}Ar/^{39}Ar ages obtained from the mylonites in the footwall suggest that their temperature was >500 °C (Harrison, 1981) just prior to 114–113 Ma. This corresponds to a cooling rate of ~30 °C/m.y. from the magmatic zircon (ca. 120 Ma) crystallization temperature of ~700 °C to hornblende closure temperature of ~500 °C.

The biotite in sample JH-75 yielded a large range of apparent ages (Fig. 4D). Observations in thin section show that the older grains are brown and deformed, whereas the younger grains are darker and undeformed. It is generally interpreted that, in nature, argon isotopes remain unfractionated during their escape from a mineral (by reheating or interaction with fluids; Kuiper, 2002). If complete argon loss occurs, then the new age indicates the timing of the end of argon loss. However, if argon loss is not complete, then the inverse isochron age will represent a geologically meaningless value between that of the initial cooling event and the end of the argon loss event (Kuiper, 2002). It is evident that the older ages (130–119 Ma) are greater than the cooling ages of hornblende from the same sample (JH-75). Therefore, we suggest that the older biotite ages have no geological meaning and that the younger ages indicate the time when argon loss was completed.

The exhumation and cooling history (Fig. 5) of the lower plate of the core complex is reconstructed on the basis of U-Pb and ^{40}Ar/^{39}Ar ages, incorporating their respective closure temperatures and constrained by the available structural data. There are no significant differences between the hornblende, muscovite, and younger biotite ages from the mylonites, indicating that the rocks cooled rapidly through the closure temperatures of all minerals (500–300 °C: Foster et al., 1990; Lovera et al., 1989, 1991; Hames and Bowring, 1994; Harrison et al., 1985; McDougall and Harrison, 1999; Vanderhaeghe et al., 2003) within only 1–2 m.y. during the Early Cretaceous. Continued cooling to ~250–200 °C (Lovera et al., 1989, 1991) is evidenced by the intercept ages of 111.2–106.5 Ma from K-feldspar samples from the lower plate of the Liaonan metamorphic core complex.

The different parts of the Liaonan metamorphic core complex show evidence for the following evolution: (1) between 128 and 121 Ma, mantle-derived dioritic and crust-derived granitic magmas were intruded into Archean–Paleoproterozoic metamorphic rocks at mid-crustal levels (Yang et al., 2004, 2007); (2) intracrustal shear and recrystallization occurred between 122–113 Ma within a thick, gently dipping extensional shear zone that brought portions of the ductile shear zone to the surface in the footwall of the Jinzhou fault.

Tectonic Implications

Several metamorphic core complexes are distributed across the North China craton (Fig. 1B). The Liaonan metamorphic core complex is the northeasternmost core complex in the North China craton and has geologic and structural features similar to those of other Early Cretaceous metamorphic core complexes in the craton (Fig. 1B) (e.g., the Yunmengshan and Huhhot metamorphic core complexes, cf. Davis et al., 2001, 2002; the Waziyu [Yiwulüshan] metamorphic core complex, cf. Darby et al., 2004; Zhang et al., 2002a, 2002b; and the Xiaoqingling metamorphic core complex, cf. Zhang et al., 1998). Widespread development of metamorphic core complexes (Fig. 1B), pull-apart basins, and regional alkaline magmatism indicates large-scale extension in the eastern North China craton during the Early Cretaceous.

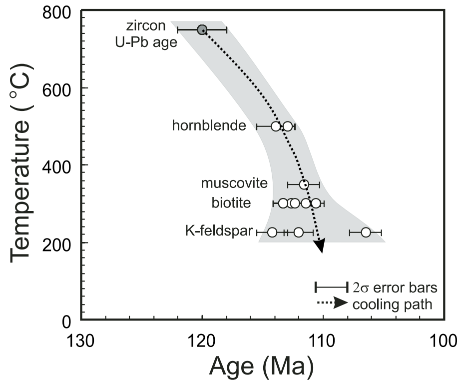

Figure 5. Reconstructed cooling history, combining the results of argon thermochronology (this study) and zircon U-Pb ages (from Wu et al., 2005).

Yin and Nie (1996) and Davies et al. (2001) suggested that all of these complexes were superposed on thickened crust resulting from earlier Mesozoic contractional events. Early Mesozoic deformation in the amalgamated North China–Mongolian plates, both contractional and extensional, occurred in an intraplate setting (Davis et al., 2001). Deformation is geographically complex, diachronous, and poorly understood. In general it is viewed as a consequence of collisional interaction between the Mongolian plates along their southern and northern margins with North China and Siberian plates, respectively. Middle to Late Jurassic deformation in the northern North China block at the latitude of the Liaonan metamorphic core complex was largely contractional with development of the east-west–trending Yanshan fold and thrust belt (Davis et al., 2001; Yang et al., 2006b). Diachronous phases of contractional deformation, accompanied by extensive magmatism, were nonsystematic in their directions of either southward or northward tectonic vergence. It is likely that the anisotropy of earlier subduction- and collision-related structures may have contributed to the diversity of the displacement sense. The amount of Mesozoic shortening across the Yanshan belt has not been adequately determined, but the involvement of crystalline basement rocks in some thrust sheets and the overturning of cover strata in the upper and lower plates of some low-angle thrusts indicate significant crustal shortening. Contraction ended in the latest Jurassic to earliest Cretaceous and was quickly followed, within a few million years in some cases, by regional northwest-southeast (NW-SE) extension over an area considerably larger than the Basin and Range province of the western United States (Davis et al., 2001; Darby et al., 2004). However, the change from north-south (N-S) contraction to NW-SE extension in the eastern North China craton during the Early Cretaceous (Li, 2000) is difficult to correlate with the N-S-directed collision between the Siberia-Mongolia-Sino-Korean plates in the Late Permian to Early Jurassic.

An alternative hypothesis is that crustal shortening and subsequent extension are related to the convergence between the Izanagi-Kula (Pacific) oceanic plates and East Asia that resulted in the accretion of terrains to the eastern edge of Asia (proto-Japan) (Engebretson et al., 1985; Isozaki, 1997; Wu et al., 2007). It is commonly believed that the eastern Pacific plate did not interact with the North China Craton until the Middle Jurassic, ca. 180–170 Ma (Wu et al., 2007). The change from a transcurrent to a convergent plate boundary with a high convergence velocity in the Late Jurassic–Early Cretaceous (Engebretson et al., 1985; Isozaki, 1997; Ratschbacher et al., 2000) induced Pacific margin backarc extension with the rollback of subducting Pacific ocean plate affecting the entire eastern Asian continental margin, including the Liaodong region. This may have caused Late Jurassic orogenically thickened crust (Davis et al., 2001; Yang et al., 2006b; Wu et al., 2007) followed by east-west (E-W) extension in the Liaonan area and throughout eastern China (Li, 2000; Wu et al., 2005). The onset of regional extension occurred in the Early Cretaceous, typically between ca. 130 and 125 Ma. It was characterized by the initiation of new normal faults, by the reactivation and inversion of some earlier thrust faults, and by the geographically widespread development of metamorphic core complexes. Extension was accompanied by large-scale I- and A-type magmatism (131–110 Ma; Wu et al., 2005; Yang et al., 2007) that presumably facilitated ductile deformation in the shear zones, and major gold mineralization throughout the easternmost North China craton (Yang et al., 2003). The high heat flow anomaly, corresponding to large-scale magmatism and gold mineralization, is explained by Early Cretaceous lithospheric thinning in the eastern North China craton (Griffin et al., 1998; Xu, 2001; Yang et al., 2003; Wu et al., 2005). All this activity triggered gravitational collapse of previously thickened crust, leading to Early Cretaceous E-W extension and formation of the Liaonan metamorphic core complex followed by rapid exhumation between 121 and 111 Ma.

CONCLUSIONS

The results of this study allow reassessment of the timing of exhumation of the Liaonan metamorphic core complex and synchronous plutonism in the eastern part of the North China craton. The Liaonan metamorphic core complex developed and cooled over a very short time span (120–107 Ma). This is supported by the initial crystallization temperature of 700 °C of zircons in syntectonic leucogranitic dikes and granitic intrusions, through to closure of argon diffusion in hornblende, muscovite, biotite, and K-feldspar (~500 to ~200 °C). The synkinematic intrusions were emplaced at 128–118 Ma, close to the time of exhumation of the metamorphic complex. The $^{40}Ar/^{39}Ar$ data on hornblende, biotite, and K-feldspar indicate that these plutons had cooled to ~200 °C by 107 Ma.

The Liaonan metamorphic core complex is the northeasternmost core complex in the North China craton and has geologic and structural features similar to those of other Early Cretaceous metamorphic core complexes in the craton (Fig. 1B). Widespread development of metamorphic core complexes, pull-apart basins, regional magmatism, and gold mineralization indicates large-scale extension in the eastern North China craton during the Early Cretaceous. This was coeval with the timing of lithospheric thinning (Yang et al., 2003, 2005). We suggest, based on the present results and published information, that Cretaceous extensional deformation and lithosphere thinning in the Liaonan area and throughout the eastern North China craton resulted from collapse of an orogenically thickened crust that was facilitated by thermal weakening due to Early Cretaceous magmatism and paleo-Pacific plate boundary reorganization.

ACKNOWLEDGMENTS

Yang is grateful to the Department of Geosciences, National Taiwan University, for a one-year Research Fellowship that allowed him to complete the analyses. We thank Terry Spell and David Moecher for their constructive reviews and Karl E. Karlstrom and Matthew Kohn for manuscript help. This work was supported by National Science Foundation grants 40672055 and 40325006. This is the Institute for Geoscientific Research (TIGeR) publication 52.

REFERENCES CITED

Chen, R.D., Li, X.D., Yang, Y.J., Zhan, L.H., Shan, X.D., and Zhang, F.S., 1999, Bedding decollement structure of the early Indosinian orogenic cycle in the south of Liaodong Peninsula: Liaoning Geology, v. 16, p. 161–169 (in Chinese).

Darby, B.J., Davis, G.A., Zhang, X.H., Wu, F.Y., Wilde, S.A., and Yang, J.H., 2004, The newly discovered Waziyu metamorphic core complex, YiwulüShan, western Liaoning Province, northwest China: Earth Science Frontiers, v. 11, p. 145–155.

Davis, G.A., and Lister, G.S., 1988, Detachment faulting in continental extension: Perspectives from the southwestern U.S: Cordillera, *in* Clark, S.P., Jr., et al., eds., Processes in continental lithospheric deformation: Geological Society of America Special Paper 218, p. 133–159.

Davis, G.A., Zheng, Y.D., Wang, C., Darby, B.J., Zhang, C.H., and Gehrels, G., 2001, Mesozoic tectonic evolution of the Yanshan fold and thrust belt, with emphasis on Hebei and Liaoning Provinces, northern China, *in* Hendrix, M.S., and Davies, G.A., eds., Paleozoic and Mesozoic tectonic evolution of central Asia: From continental assembly to intracontinental deformation: Geological Society of America Memoir 194, p. 171–198.

Davis, G.A., Darby, B.J., Zheng, Y., and Spell, T.L., 2002, Geometric and temporal evolution of an extensional detachment fault, Hohhot metamorphic core complex, Inner Mongolia, China: Geology, v. 30, p. 1003–1006, doi: 10.1130/0091-7613(2002)030<1003:GATEOA>2.0.CO;2.

Engebretson, D.C., Cox, A., and Gordon, R.G., 1985, Relative motion between oceanic and continental plates in the Pacific basin: Geological Society of America Special Paper 206, 59 p.

Foster, D.A., Harrison, T.M., Copeland, P., and Heizler, M.T., 1990, Effects of excess Ar on K-feldspar age spectra in the presence of large diffusion domains and plagioclase inclusions: Geochimica et Cosmochimica Acta, v. 54, p. 1699–1706, doi: 10.1016/0016-7037(90)90401-6.

Fowler, T.K., Jr., and Paterson, S.R., 1997, Timing and nature of magmatic fabrics from structural relations around stoped blocks: Journal of Structural Geology, v. 19, p. 209–224, doi: 10.1016/S0191-8141(96)00058-2.

Gang, J., Han, X., and Wang, F., 1999, Structural deformation and evolution of Archean palaeocontinental crust in south Liaoning: Liaoning Geology, v. 16, p. 121–127.

Griffin, W.L., Zhang, A., O'Reilly, S.Y., and Ryan, C.G., 1998, Phanerozoic evolution of the lithosphere beneath the Sino-Korean Craton, *in* Flower, M.F.J., et al., eds., Mantle dynamics and plate interaction in East Asia: American Geophysical Union Geodynamics Series 27, p. 107–126.

Guo, C.L., Wu, F.W., Yang, J.H., Lin, J.Q., and Sun, D.Y., 2004, The extensional setting of the Early Cretaceous magmatism in eastern China: Example from the Yinmawanshan pluton in southern Liaodong Peninsula: Acta Petrologica Sinica, v. 20, p. 1193–1204.

Hames, W.E., and Bowring, S.A., 1994, An empirical evaluation of the argon diffusion geometry in muscovite: Earth and Planetary Science Letters, v. 124, p. 161–169, doi: 10.1016/0012-821X(94)00079-4.

Harrison, T.M., 1981, Diffusion of ^{40}Ar in hornblende: Contributions to Mineralogy and Petrology, v. 70, p. 324–331.

Harrison, T.M., Duncan, I., and McDougall, I., 1985, Diffusion of ^{40}Ar in biotite: Temperature, pressure and compositional effects: Geochimica et Cosmochimica Acta, v. 49, p. 2461–2468, doi: 10.1016/0016-7037(85)90246-7.

Isozaki, Y., 1997, Jurassic accretion tectonics of Japan: The Island Arc, v. 6, p. 25–51, doi: 10.1111/j.1440-1738.1997.tb00039.x.

Kuiper, Y.D., 2002, The interpretation of inverse isochron diagrams in $^{40}Ar/^{39}Ar$ geochronology: Earth and Planetary Science Letters, v. 203, p. 499–506, doi: 10.1016/S0012-821X(02)00833-6.

Li, X.H., 2000, Cretaceous magmatism and lithospheric extension in southeast China: Journal of Asian Earth Sciences, v. 18, p. 293–305, doi: 10.1016/S1367-9120(99)00060-7.

Liaoning Bureau of Geology and Mineral Resources, 1989, Regional geology of Liaoning Province: Beijing, Geological Publishing House (in Chinese with English summary), 856 p.

Lister, G.S., and Davis, G.A., 1989, The origin of metamorphic core complex and detachment faults formed during extension in the northern Colorado River region, USA: Journal of Structural Geology, v. 11, p. 65–94, doi: 10.1016/0191-8141(89)90036-9.

Liu, D.Y., Nutman, A.P., Compston, W., Wu, J.S., and Shen, Q.H., 1992, Remnants of ≥3800 Ma crust in the Chinese part of the Sino-Korean craton: Geology, v. 20, p. 339–342, doi: 10.1130/0091-7613(1992)020<0339:ROMCIT>2.3.CO;2.

Liu, J., Davis, G.A., Lin, Z., and Wu, F., 2005, The Liaonan metamorphic core complex, Southeastern Liaoning Province, North China: A likely contributor to Cretaceous rotation of Eastern Liaoning, Korea and contiguous areas: Tectonophysics, v. 407, p. 65–80, doi: 10.1016/j.tecto.2005.07.001.

Lovera, O.M., Richter, F.M., and Harrison, T.M., 1989, The $^{40}Ar/^{39}Ar$ thermochronometry for slowly cooled samples having a distribution of diffusion domain sizes: Journal of Geophysical Research, v. 94, p. 17,917–17,935.

Lovera, O.M., Richter, F.M., and Harrison, T.M., 1991, Diffusion domains determined by ^{39}Ar released during step-heating: Journal of Geophysical Research, v. 96, p. 2057–2069.

Lu, X.P., Wu, F.Y., Lin, J.Q., Sun, D.Y., Zhang, Y.B., and Guo, C.L., 2004, Geochronological framework of Precambrian magmatism in the southern Liaodong Peninsula: Constraints on the crustal evolution of North China Craton: Scientia Geologica Sinica, v. 39, p. 123–138.

Luo, Y., Sun, M., Zhao, G.C., Li, S.Z., Ye, K., and Xia, X.P., 2004, LA-ICP-MS U-Pb zircon ages of the Liaohe Group in the Eastern Block of the North China Craton: Constraints on the evolution of the Jiao-Liao-Ji Belt: Precambrian Research, v. 134, p. 349–371, doi: 10.1016/j.precamres.2004.07.002.

McDougall, I., and Harrison, T.M., 1999, Geochronology and thermochronology by the $^{40}Ar/^{39}Ar$ method: New York, Oxford, Oxford University Press, 269 p.

Meng, Q.R., 2003, What drove late Mesozoic extension of the northern China-Mongolia tract: Tectonophysics, v. 369, p. 155–174, doi: 10.1016/S0040-1951(03)00195-1.

Menzies, M.A., Fan, W.M., and Zhang, M., 1993, Palaeozoic and Cenozoic lithoprobes and the loss of >120 km of Archean lithosphere, Sino-Korean craton, China, *in* Prichard, H.M., et al., eds., Magmatic processes and plate tectonics: Geological Society [London] Special Publication 76, p. 71–81.

Passchier, C.W., and Trouw, R.A.J., 1998, Microtectonics (second edition): Heidelberg, Springer Verlag, 289 p.

Ratschbacher, L., Hacker, B.R., Webb, L.E., McWilliams, M., Ireland, T., Dong, S., Calvert, A., Chateigner, D., and Wenk, H.R., 2000, Exhumation of the ultrahigh-pressure continental crust in east central China: Cretaceous and Cenozoic unroofing and the Tan-Lu fault: Journal of Geophysical Research, v. 105, B6, p. 13,303–13,338, doi: 10.1029/2000JB900040.

Renne, P.R., Swisher, C.C., Deino, A.L., Karner, D.B., Owens, T.L., and DePaolo, D.J., 1998, Intercalibration of standards, absolute ages and uncertainties in $^{40}Ar/^{39}Ar$ dating: Chemical Geology, v. 145, p. 117–152, doi: 10.1016/S0009-2541(97)00159-9.

Vanderhaeghe, O., Teyssier, C., McDougall, I., and Dunlap, W.J., 2003, Cooling and exhumation of the Shuswap metamorphic core complex constrained by $^{40}Ar/^{39}Ar$ thermochronology: Geological Society of America Bulletin, v. 115, p. 200–216.

Wang, H.Z., and Mo, X.X., 1996, An outline of the tectonic evolution of China: Episodes, v. 18, p. 6–16.

Wendt, I., and Carl, C., 1991, The statistical distribution of the mean squared weighted mean: Chemical Geology, v. 86, p. 275–285.

Wu, F.Y., Lin, J.Q., Wilde, S.A., Zhang, X.O., and Yang, J.H., 2005, Nature and significance of Early Cretaceous giant igneous event in eastern China: Earth and Planetary Science Letters, v. 233, p. 103–119, doi: 10.1016/j.epsl.2005.02.019.

Wu, F.Y., Yang, J.H., Lo, C.H., Wilde, S.A., Sun, D.Y., and Jahn, B.M., 2007, The Jiamusi Massif: A Jurassic accretionary terrane along the western Pacific margin of NE China: The Island Arc, v. 16, p. 156–172, doi: 10.1111/j.1440-1738.2007.00564.x.

Xu, Y.G., 2001, Thermo-tectonic destruction of the Archean lithospheric keel beneath the Sino-Korean Craton in China: Evidence, timing and mechanism: Physics and Chemistry of the Earth, v. 26, p. 747–757, doi: 10.1016/S1464-1895(01)00124-7.

Xu, Z.Q., Li, H., Wang, Z., and Li, D., 1991, Crustal contraction and extension in Southern Liaoning: Geological Review, v. 37, p. 193–202 (in Chinese).

Yang, J.H., Wu, F.W., and Wilde, S.A., 2003, A review of geodynamic setting of large-scale late Mesozoic gold mineralization in the North China Craton: An association with lithospheric thinning: Ore Geology Reviews, v. 23, p. 125–152, doi: 10.1016/S0169-1368(03)00033-7.

Yang, J.H., Wu, F.Y., Chung, S.L., Wilde, S.A., and Chu, M.F., 2004, Multiple sources for the origin of granites: Geochemical and Nd/Sr isotopic evidence from the Gudaoling granite and its mafic enclaves, NE China: Geochimica et Cosmochimica Acta, v. 68, p. 4469–4483, doi: 10.1016/j.gca.2004.04.015.

Yang, J.H., Chung, S.L., Wilde, S.A., Wu, F.Y., Chu, M.F., Lo, C.H., and Fan, H.R., 2005, Petrogenesis of Early Cretaceous intrusions in the Sulu ultrahigh-pressure orogenic belt, east China and their relationship to lithospheric thinning: Chemical Geology, v. 222, p. 200–231, doi: 10.1016/j.chemgeo.2005.07.006.

Yang, J.H., Wu, F.Y., Chung, S.L., Wilde, S.A., and Chu, M.F., 2006a, A hybrid origin for the Qianshan A-type granite, northeast China: Geochemical and Sr-Nd-Hf isotopic evidence: Lithos, v. 89, p. 89–106, doi: 10.1016/j.lithos.2005.10.002.

Yang, J.H., Wu, F.Y., Shao, J.A., Wilde, S.A., Xie, L.W., and Liu, X.M., 2006b, Constraints on the timing of the Yanshan Fold and Thrust Belt, North China: Earth and Planetary Science Letters, v. 246, p. 336–352, doi: 10.1016/j.epsl.2006.04.029.

Yang, J.H., Wu, F.Y., Wilde, S.A., Xie, L.W., Yang, Y.H., and Liu, X.M., 2007, Trace magma mixing in granite genesis: In-situ U-Pb dating and Hf-isotope analysis of zircons: Contributions to Mineralogy and Petrology, v. 153, p. 177–190, doi: 10.1007/s00410-006-0139-7.

Yang, Z., Meng, Q., Gang, J., and Han, X., 1996, The metamorphic core complex structure in south Liaoning: Liaoning Geology, v. 13, p. 241–250.

Yin, A., and Nie, S., 1996, A Phanerozoic palinspastic reconstruction of China and its neighboring regions, *in* Yin, A., and Harrison, T.A., eds., The tectonic evolution of Asia: New York, Cambridge University Press, p. 442–485.

Zeng, L., and Li, H., 1996, Structural deformation and fluid process in Jinzhou uplifting region, southern Liaoning Province: Geological Journal of China Universities, v. 2, p. 155–164 (in Chinese).

Zhang, H., and Wang, X., 1995, Reunderstanding on the geological structure of Jinzhou Region in southern Liaoning Province: Liaoning Geology, v. 12, p. 33–40 (in Chinese).

Zhang, J.J., Zheng, Y.D., and Liu, S.W., 1998, Structure, mechanism and tectonic evolution of Xiaoqinling Metamorphic Core Complex: Beijing, Oceanic Press, p. 1–120 (in Chinese).

Zhang, S.H., Zhao, Y., and Song, B., 2006, Hornblende thermobarometry of the Carboniferous granitoids from the Inner Mongolia Paleo-uplift: Implications for the tectonic evolution of the northern margin of North China block: Mineralogy and Petrology, v. 87, p. 123–141, doi: 10.1007/s00710-005-0116-2.

Zhang, X.H., Li, T.S., Pu, Z.P., and Wang, H., 2002a, ^{40}Ar-^{39}Ar ages of Louzidian-Dachengzi ductile shear zone near Chifeng, Inner Mongolia and their tectonic significance: Chinese Science Bulletin, v. 47, p. 1292–1297, doi: 10.1360/02tb9287.

Zhang, X.H., Li, T.S., and Pu, Z.P., 2002b, ^{40}Ar-^{39}Ar thermochronology of two ductile shear zone from Yiwulüshan, West Liaoning region: Age constraints on the Mesozoic tectonic events: Chinese Science Bulletin, v. 47, p. 1113–1118, doi: 10.1360/02tb9250.

Zhao, G.C., Wilde, S.A., Cawood, P.A., and Sun, M., 2001, Archean blocks and their boundaries in the North China Craton: Lithological, geochemical, structural and P-T path constraints and tectonic evolution: Precambrian Research, v. 107, p. 45–73, doi: 10.1016/S0301-9268(00)00154-6.

Manuscript Received 31 July 2006
Revised Manuscript Received 28 May 2007
Manuscript Accepted 14 June 2007

Printed in the USA